Original Research

Hot deformation behavior and flow stress modeling of annealed AZ61 Mg alloys

Chinghao Liao[a], Horngyu Wu[b,*], Chengtao Wu[b], Fengjun Zhu[b], Shyong Lee[a]

[a]Department of Mechanical Engineering, National Central University, 300, Jhongda Road, Jhongli 320, Chinese Taipei
[b]Department of Mechanical Engineering, Chung Hua University, 707, Sec. 2, WuFu Road, HsinChu 300, Chinese Taipei

Abstract

In this study, the hyperbolic-sine type constitutive equation was used to model the flow stress of annealed AZ61 magnesium (Mg) alloys. Hot compression tests were conducted at the temperatures ranging from 250 °C to 450 °C and at the strain rates ranging from 1×10^{-3} s^{-1} to 1 s^{-1} on a Gleeble-3500 thermo-simulation machine. Constitutive equations as a function of strain were established through a simple extension of the hyperbolic sine constitutive relation. The effects of annealing heat treatments on the variations in constitutive parameters with strain were discussed. The hot compressive flow curves exhibited typical features of dynamic recrystallization. Multiple peak flow curves were observed in the annealed specimens upon testing at a strain rate of 1×10^{-1} s^{-1} and at various temperatures. Variations in constitutive parameters with strain were related to flow behavior and dependent on the initial conditions of the test specimens. The flow stresses of annealed AZ61 Mg alloys were predicted well by the strain-dependent constitutive equations of the hyperbolic sine function under the deformation conditions employed in this study.
© 2014 Chinese Materials Research Society. Production and hosting by Elsevier B.V. All rights reserved.

1. Introduction

Magnesium (Mg) is one of the lightest structural metals. Replacing aluminum and steel with Mg in equal volumes will result in weight savings of approximately 33% and 77%, respectively. The remarkable weight-saving capability of Mg and its alloys offers significant potential for the manufacturing of portable and automotive components. However, the use of wrought Mg alloys has so far been limited, partly because of the low formability of such alloys at room temperature. This poor formability at room temperature is attributed to the hexagonal close-packed crystal structure of these alloys, which results in limited slip systems [1]. Therefore, the metalworking processes of wrought Mg alloys are always performed at elevated temperatures, which non-basal slips can be activated to enhance plastic formability [2].

During the hot forming process, an Mg alloy is liable to undergo strain hardening, activation of non-basal slip systems [1], grain growth [3,4], dynamic recovery [5], and dynamic recrystallization (DRX) [6–11]. These metallurgical phenomena result in changes in the microstructure, thus resulting in variations of flow behavior during hot deformation. Understanding the flow behavior of Mg alloys under hot deformation conditions is of great importance in designing hot bulk metal forming processes because of the effect of such behavior on the metal flow pattern. Constitutive relationships are often used to describe the plastic flow properties of metals and alloys in a form that can be used for the numerical modeling of hot working processes.

*Corresponding author. Tel.: +886 3 5186493; fax: +886 3 5186521.
E-mail addresses: whitemoon0926@gmail.com (C. Liao), ncuwu@chu.edu.tw (H. Wu), cool780207@hotmail.com (C. Wu), b09627016@chu.edu.tw (F. Zhu), shyong@cc.ncu.edu.tw (S. Lee).

The constitutive behavior of various metals and alloys has been investigated using different analytical, phenomenological, and empirical models [12–25]. A critical review of experimental results and constitutive descriptions for metals and alloys in hot working has been reported by Lin and Chen [12], who indicated that the phenomenological models do not consider a detailed understanding of the physical phenomena involved in the deformation process. Thus, more attention should be directed toward the coupling effects of the processing parameters on the flow behavior when developing constitutive models. Physical-based models consider the thermal deformation mechanism of metal in the deformation process, but the complexities of these models limit their use in the commercial finite element simulation. Artificial neural network (ANN) models provide an efficient alternative, but the modeling offers no physical insight. Lin et al. [15] proposed a two-stage constitutive model based on the stress–dislocation relation and kinetics of DRX to calculate the flow stress of a nickel-based superalloy. A revised model incorporating the effects of the flow stress, strain rate, and temperature of 42CrMo steel at elevated temperatures was derived through the compensation of strain and strain rate, as reported by Lin et al. [16]. Slooff et al. [17] introduced a strain-dependent parameter to the hyperbolic sine constitutive equation to calculate the flow stress of three as-extruded AZ series Mg alloys. The strain-dependent constitutive equation used to predict the flow stress of an as-extruded AZ61 Mg alloy was developed by Slooff et al. [18]. Changizian et al. [21] investigated the high-temperature flow behavior modeling of a homogenized AZ81 Mg alloy considering the coupled effects of strain, strain rate, and temperature. Sabokpa et al. [22] explored the high-temperature flow behavior of an AZ81 Mg alloy using artificial neural network modeling. Yu et al. [23] reported on the strain-dependent constitutive analysis of hot deformation and hot workability of a T4-treated ZK60 Mg alloy. Constitutive analyses of an as-extruded AZ61 Mg alloy using constant and strain-dependent stress multipliers were presented by Liao et al. [24]. Hot compressive flow stress modeling of a homogenized AZ61 Mg alloy using strain-dependent constitutive equations was reported by Wu et al. [25]. However, the effect of annealing heat treatment on flow behavior and constitutive analysis has not been assessed in previous research.

Annealing heat treatment is invariably introduced to eliminate the effects of cold working. Such treatment can induce ductility, soften the material, relieve internal stresses, alter the microstructure, and improve workability. Therefore, annealing influences the hot deformation characteristics of the material, as well as the constitutive relationship. Constitutive analysis of as-extruded AZ61 Mg alloys was performed in a previous study [24]. In this work, annealed AZ61 Mg alloys are investigated to clarify the influence of annealing heat treatment on hot deformation behavior. This work focuses on the effect of annealing heat treatment on hot deformation characteristics and constitutive parameters. Based on the measured flow stress, the constitutive equations were established as a function of strain. In addition, the fundamental scientific points, such as the effects of annealing on the deformation behavior and the constitutive parameters in extruded AZ61 Mg alloys, were discussed.

2. Materials and experimental procedures

The experimental material was an extruded AZ61 Mg alloy rod with an analyzed chemical composition of Mg-6.1Al-1.1Zn-0.18Mn (wt%), as measured by induction-coupled plasma and spark optical emission spectrometry apparatuses. The cylindrical cast ingot with a diameter of 240 mm was extruded into a 90 mm diameter rod with an extrusion ratio of 7 at a billet preheating temperature of 300 °C. Cylindrical specimens with a height of 12 mm and a diameter of 8 mm were machined from the extruded rod along the axial direction for the compression tests. ASTM E209 standard was used as the reference for the compression test. The specimens were annealed at 300 °C for 30 min and at 400 °C for 60 min before hot deformation. Isothermal hot compression tests were conducted using a Gleeble 3500 thermal simulation machine at temperatures ranging from 250 °C to 450 °C and at constant strain rates between 1×10^{-3} s^{-1} and 1 s^{-1}. The stimulator was equipped with a control system to induce the exponential decay of the actuator speed to obtain a constant strain rate. Graphite foils were used to reduce the friction between the punch and specimen interfaces. The deformation temperature was measured using thermocouples that were spot-welded to the outer surface at the central region along the height of the specimen. Before being subjected to hot compression, the specimens were heated until the deformation temperature was reached. The deformation temperature was then kept constant for 3 min to eliminate thermal gradients and to ensure the uniform temperature of the specimens. The decrease in height at the end of the compression tests was approximately 50%, which corresponds to a true strain of approximately 0.7. The specimens were subsequently quenched in water to retain the microstructures after being subjected to hot compression. The true stress–true strain curves were constructed using the load–stroke data obtained from the compression tests.

3. Results and discussion

3.1. Annealing heat treatment

The effects of annealing parameters on the variations in the hardness of the test specimens are given in Fig. 1. Hardness generally decreases with increasing annealing time at both temperatures. No significant decrease in hardness values was observed for annealing times longer than 30 and 60 min at 300 and 400 °C, respectively. Therefore, 300 °C–30 min and 400 °C–60 min were selected as the annealing heat treatment conditions in this work.

Fig. 2 shows the initial microstructures of the test AZ61 Mg alloys annealed at 300 °C–30 min and 400 °C–60 min. The microstructure of the as-extruded specimen is also given for comparison. The as-extruded specimen had a bimodal grain size structure consisting of coarse deformed grains and fine recrystallized grains (Fig. 2a). Fig. 2b shows that annealing at 300 °C for 30 min caused recrystallization and reduced the size of the as-extruded coarse grains. Significant grain growth occurred upon annealing at 400 °C for 60 min, as shown
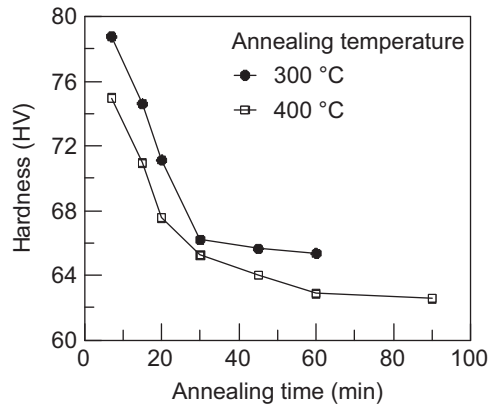
Fig. 1. Variations in specimen hardness with annealing time at two temperatures.

in Fig. 2c. However, a more uniform grain distribution was observed in the microstructure of the 400 °C annealed specimen. The variations in the initial microstructures that resulted from annealing heat treatments should influence the hot deformation behavior and constitutive relationship.

AZ61 Mg alloy is a commercially available Mg alloy composed of aluminum (nominally 6 wt%), zinc (nominally 1 wt%), and other trace elements. At 6 wt% Al, the Mg-Al phase diagram [26] indicates that AZ61 Mg alloy exhibits two phase structures at temperatures below approximately 305 °C. These structures consist of an Mg-rich solid solution and an intermetallic compound $Mg_{17}Al_{12}$ phase. The AZ61 Mg alloy exhibits a single phase of Mg-rich solid solution at temperatures ranging from approximately 305 °C to 540 °C. Therefore, annealing AZ61 Mg alloys at different temperatures influences the state of the $Mg_{17}Al_{12}$ phase. Fig. 3 shows the existence of an elongated intermetallic compound $Mg_{17}Al_{12}$ phase in the slightly etched optical microstructures of the as-extruded and 300 °C annealed specimens, whereas only a few such particles were found in the 400 °C annealed specimen. Energy dispersive spectrometer analysis of the specimens revealed that Al atoms are mainly contained in the deformed particles, as shown in Fig. 4. Thus, variations in the initial microstructures and the status of the intermetallic compound $Mg_{17}Al_{12}$ phase in the annealed AZ61 Mg alloys affect the hot deformation behavior.

3.2. True stress–strain curves

Figs. 5 and 6 respectively show the true stress–strain curves of the specimens annealed at 300 and 400 °C under various deformation conditions. The overall level of the flow curve decreases when the strain rate is decreased and/or the temperature is increased for both annealed specimens. At low temperatures, flow stress initially increases because of strain hardening and reaches a peak value, subsequently decreasing when the strain is increased. The features of the flow curves indicate that DRX occurs during hot deformation [19,20,24,25]. The rates of strain hardening and strain softening vary with the deformation conditions. Flow stress is a
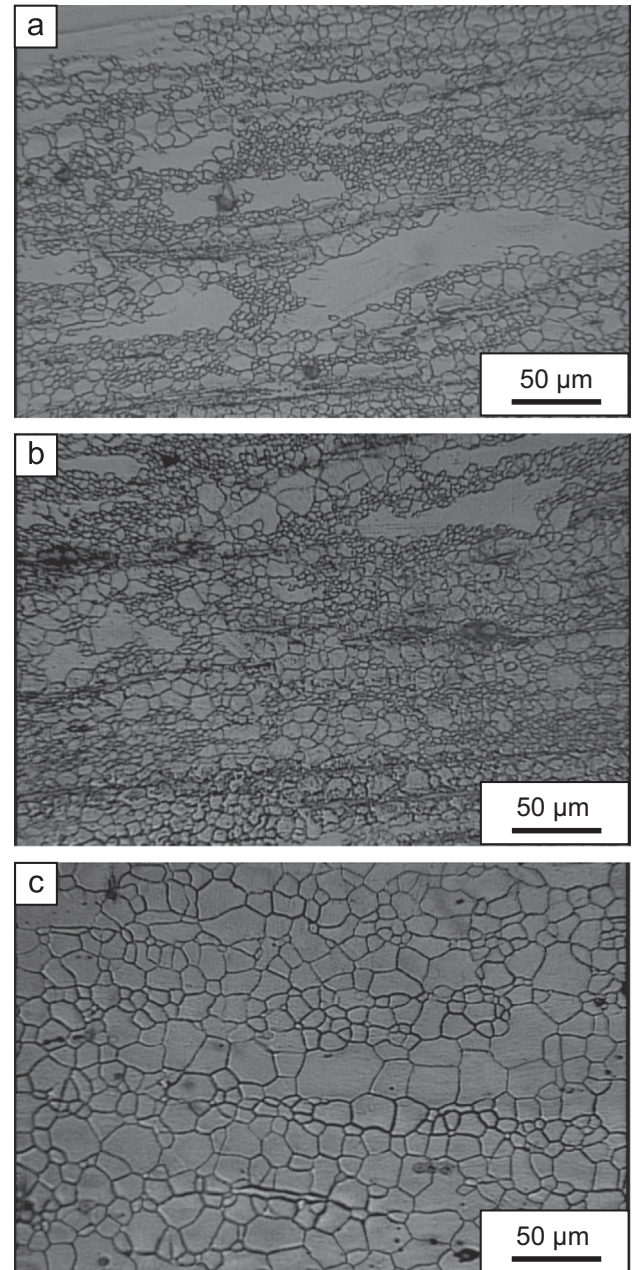

Fig. 2. Initial microstructures of the (a) as-extruded, (b) 300 °C annealed, and (c) 400 °C annealed AZ61 Mg alloys.

function of dislocation density during deformation. The initial rapid increase in stress is associated with the increase in dislocation density, which results in strain hardening. At lower strain rates, dislocation multiplication is less rapid and contributes to a lower strain hardening effect than that at higher strain rates. Deformation at higher temperatures and/or at lower strain rates can result in higher DRX kinetics because of higher diffusivity at higher temperatures and/or more time for nucleation and growth of DRX. Thus, a lower strain hardening effect is observed at higher temperatures and/or lower strain rates.

Fig. 7 shows the variations in the peak stress and peak strain as a function of temperature at various strain rates. The peak
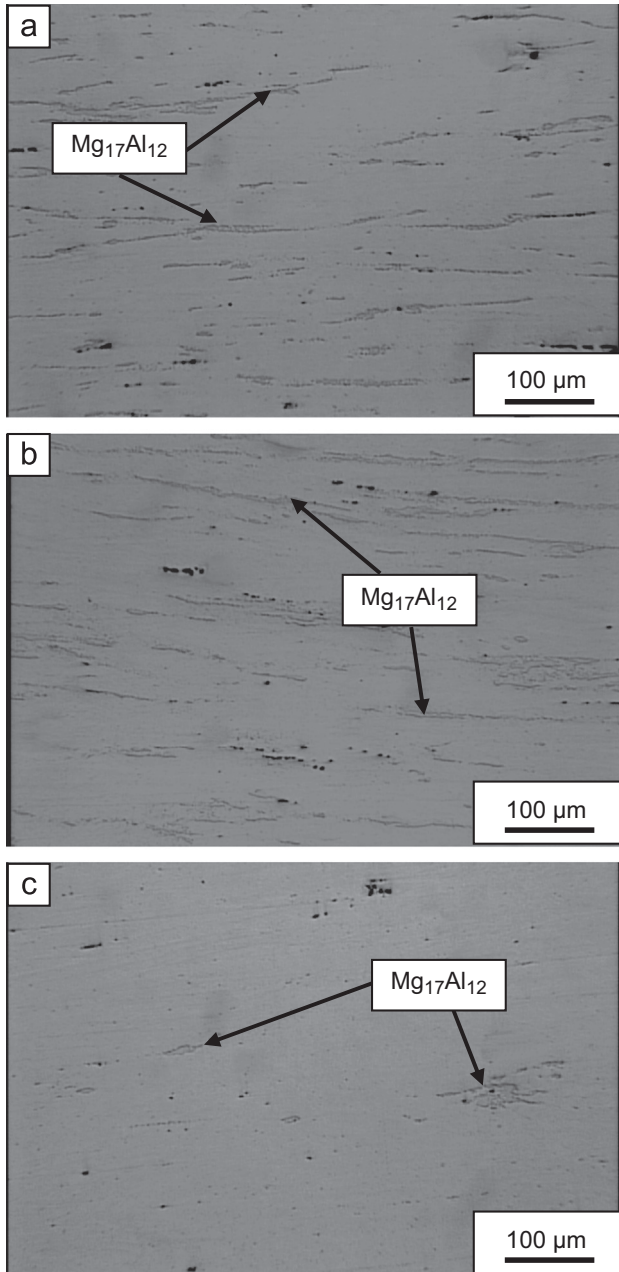
Fig. 3. Optical microstructures of the slightly etched (a) as-extruded, (b) 300 °C annealed, and (c) 400 °C annealed AZ61 Mg alloys.
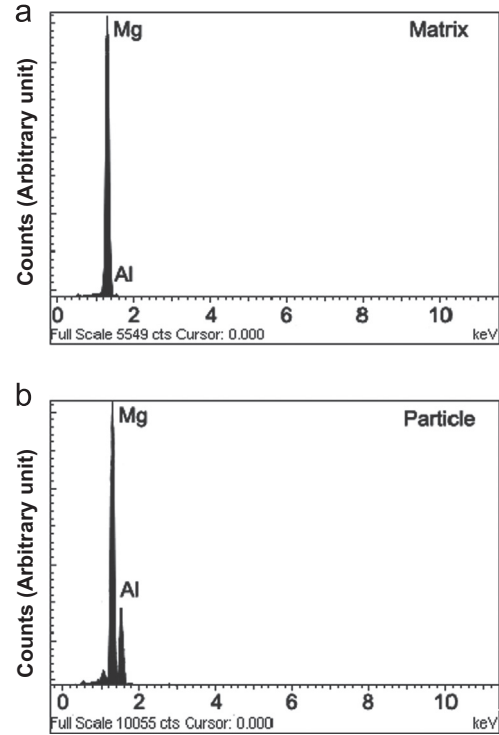

Fig. 4. EDS analyses of the (a) Mg-rich solid solution matrix and (b) deformed particles presented in the microstructures of the AZ61 Mg alloys.

Fig. 5. Compression curves for the 300 °C annealed AZ61 Mg alloy during hot deformation at (a) a temperature of 300 °C and (b) a strain rate of 1×10^{-3} s^{-1}.

stress and peak strain are evidently dependent on the strain rate and temperature. The peak stress and peak strain increase with increasing strain rate at a fixed temperature. Moreover, these parameters increased with decreasing temperature at a given strain rate. Similar results were reported by Zhou et al. [27]. Fig. 7a shows that the peak stresses of the 400 °C annealed specimens are higher than those of the 300 °C annealed specimens. The flow curves in the 400 °C annealed specimens reach peak stresses at strains greater than those in the 300 °C annealed specimens (Fig. 7b). The varying flow behavior observed between the 400 and 300 °C annealed specimens under the same deformation conditions should be related to the
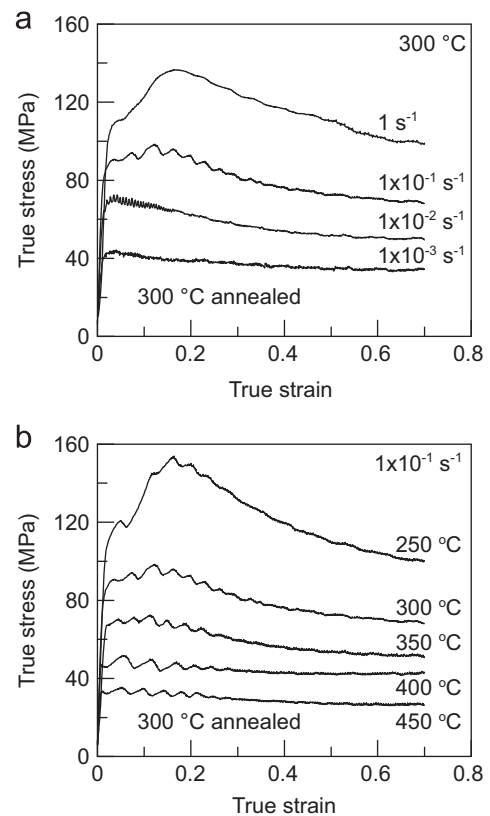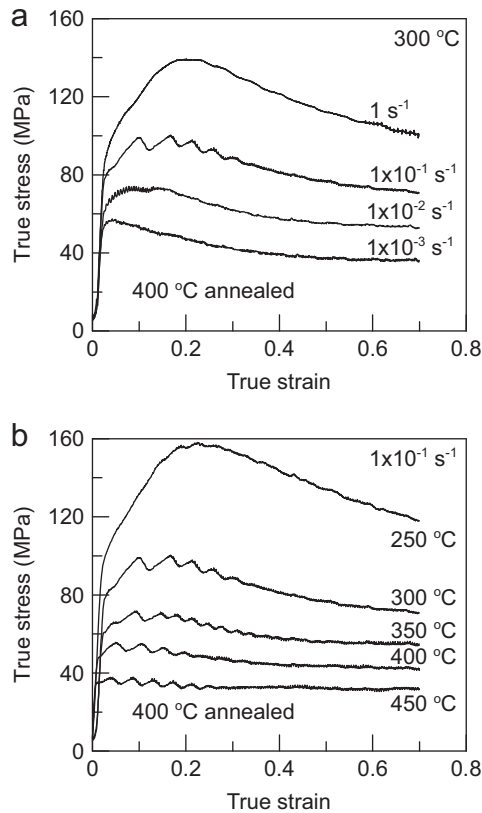
Fig. 6. Compression curves for the 400 °C annealed AZ61 Mg alloy during hot deformation at (a) a temperature of 300 °C and (b) a strain rate of 1×10^{-3} s^{-1}.

Fig. 7. (a) Peak stress and (b) peak strain as a function of temperature at various strain rates.

variations in microstructural changes during hot deformation, resulting from different initial microstructures. Peak stress in the compressive flow curve is the point at which strain hardening rate is balanced by the dynamic softening rate. In materials with DRX during hot deformation, DRX rate influences the values of peak stress and peak strain. As indicated by Roberts [28], the DRX rate decreases with increasing initial grain size. Therefore, lower DRX rates in the 400 °C annealed specimens result in greater peak stresses and peak strains than those in the 300 °C annealed specimens.

Fig. 8 shows the microstructures of the 300 and 400 °C annealed specimens deformed under different conditions. The microstructures indicate that DRX occurs during hot compression. The 300 °C annealed specimens exhibit a smaller average grain size of DRX than that of the 400 °C annealed specimens under the same deformation conditions. As shown in Fig. 3, annealing at 400 °C decreases the amount of $Mg_{17}Al_{12}$ particles to pin the recrystallized grain boundaries, thus resulting in a larger grain size of DRX.

The main difference in the flow curves for the as-extruded and annealed AZ61 Mg alloy specimens is the stress–strain behavior. Monotonic stress behavior was observed in the as-extruded AZ61 Mg alloys [17–19,24], in which a single peak stress was observed in the stress–strain relationship. However, multiple peak stress behavior was observed in the annealed AZ61 Mg alloy specimens. The stress–strain curves at low
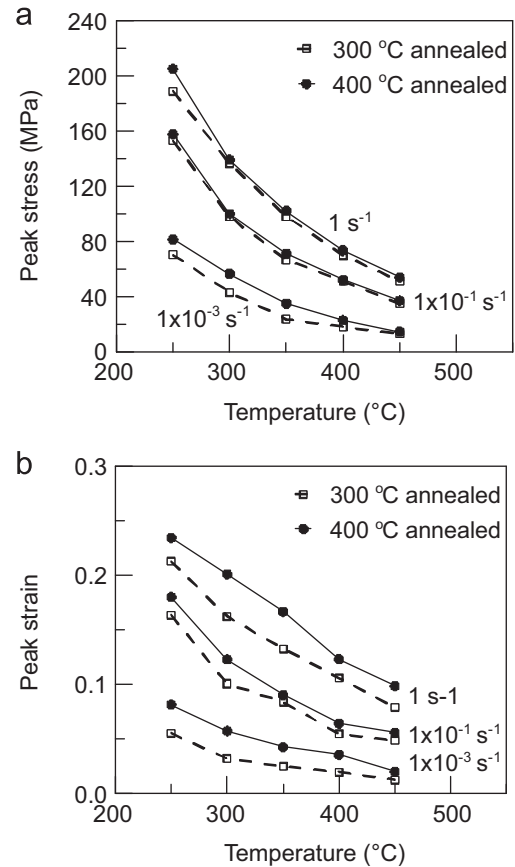
strains display multiple peaks in the stress upon deforming at a strain rate of 1×10^{-1} s^{-1} and at various temperatures. The occurrence of DRX with multiple peak flow behavior under constant strain rate conditions has been reported in various metals and alloys [29–32].

In the classic approach to DRX, which is the model proposed by Luton and Sellars [33], the stress–stress curve manifests single peak or multiple peak flow behavior depending on the ratio of the peak strain (the strain associated with the first peak stress) to the recrystallization strain (the strain required for a large fraction of DRX to occur). The peak strain can be replaced by the critical strain (the strain to initiate DRX) in some cases [34]. In another model proposed by Sakai et al. [35,36], the multiple peak flow curve is associated with a nucleation control and impingement mechanism (i.e., grain coarsening), and the initial grain size is usually less than twice the steady-state DRX grain size. The microstructures of the annealed specimens deformed at 1×10^{-1} s^{-1} and at various temperatures (Figs. 8c–f) do not exhibit the phenomenon of grain coarsening. These observations indicate that the multiple peak flow behavior observed in the annealed specimens do not meet the criterion proposed by Sakai et al. [35,36].

The stress–strain curve is generally believed to exhibit multiple peaks at low strains under the deformation conditions of a low strain rate and/or a high temperature. The curve
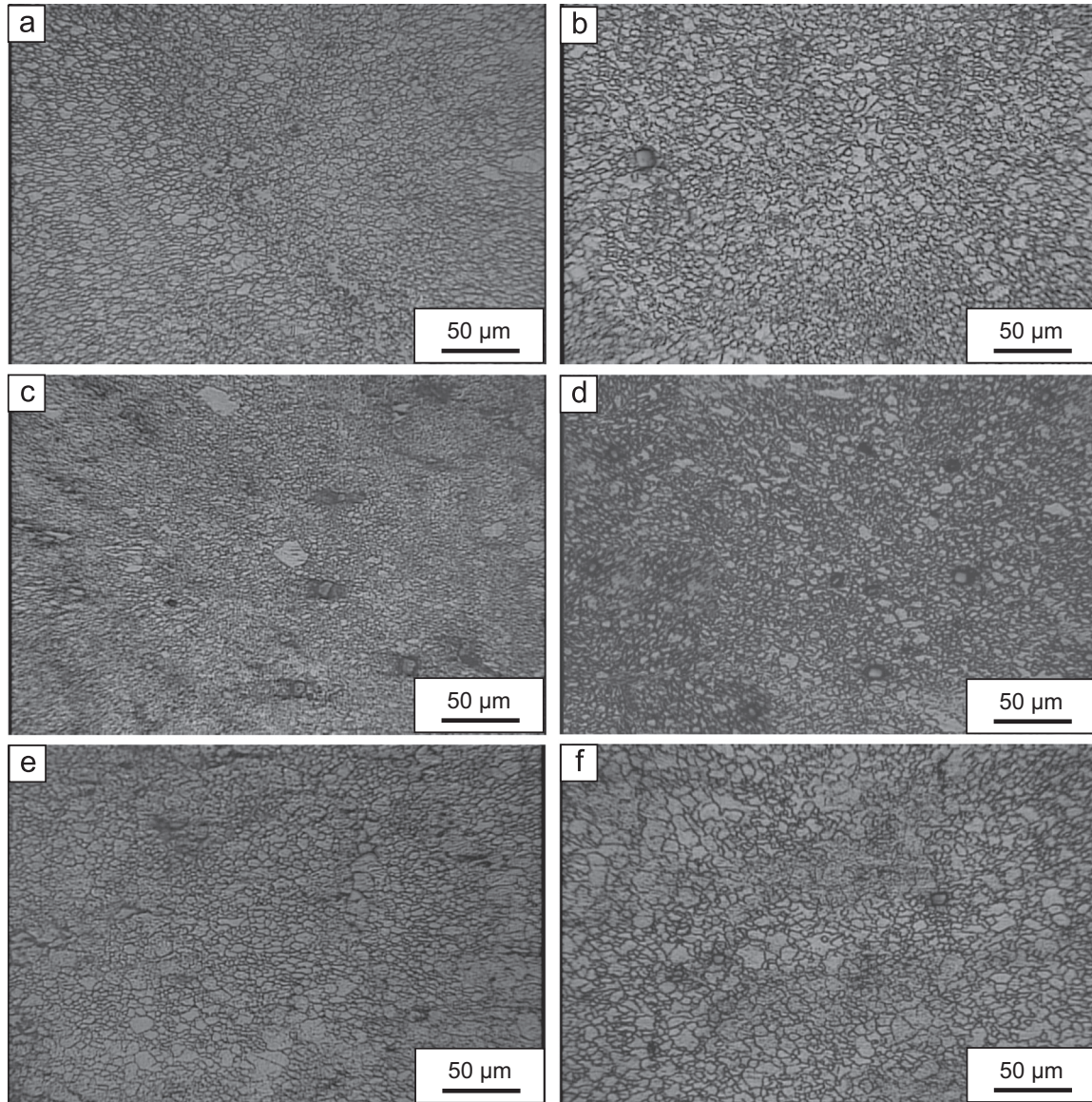
Fig. 8. Optical microstructures of the hot compressed 300 °C annealed (left side) and 400 °C annealed (right side) specimens deformed at (a and b) 1×10^{-3} s^{-1} and 300 °C, (c and d) 1×10^{-1} s^{-1} and 350 °C, and (e and f) 1×10^{-1} s^{-1} and 400 °C.

gradually becomes flat at high strains, but the stress–strain curve is smooth with only one single peak at a high strain rate and/or a low temperature [35,37]. However, the annealed AZ61 Mg specimens do not reveal multiple peak flow behavior under similar deformation conditions in this work. The multiple peak flow behavior occurred mainly under the deformation conditions of a strain of 1×10^{-1} s^{-1} and at various temperatures. Various DRX mechanisms, such as twin DRX [38,39], low-temperature DRX [40], continuous DRX [41], discontinuous DRX [42], and rotational DRX [43], have been reported in Mg alloys. Thus, the multiple peak flow behavior found in the annealed specimens may result from complex DRX mechanisms, variation in the initial microstructure, and the status of the $Mg_{17}Al_{12}$ particles. Further study is required to explore the possible reasons for the multiple peak flow behavior in annealed AZ61 Mg alloys.

3.3. Constitutive analysis

Constitutive equations including an Arrhenius term have been commonly applied to metals and alloys to the calculate flow stress during hot working processes. The function relating stress and strain rate is generally the hyperbolic-sine [44] because the power and exponential laws lose linearity at high and low stresses, respectively. The hyperbolic sine-type equation is generally expressed as

$$\dot{\varepsilon} = A[\sinh(\alpha\sigma)]^n \exp\left[\frac{-Q}{RT}\right], \tag{1}$$

where A (s^{-1}) and α (MPa^{-1}) are constants, σ is the flow stress (MPa), n is the stress exponent, R is the universal gas constant, T is the absolute temperature (K), and Q is the activation energy (kJ mol^{-1}). The rate-controlling mechanism
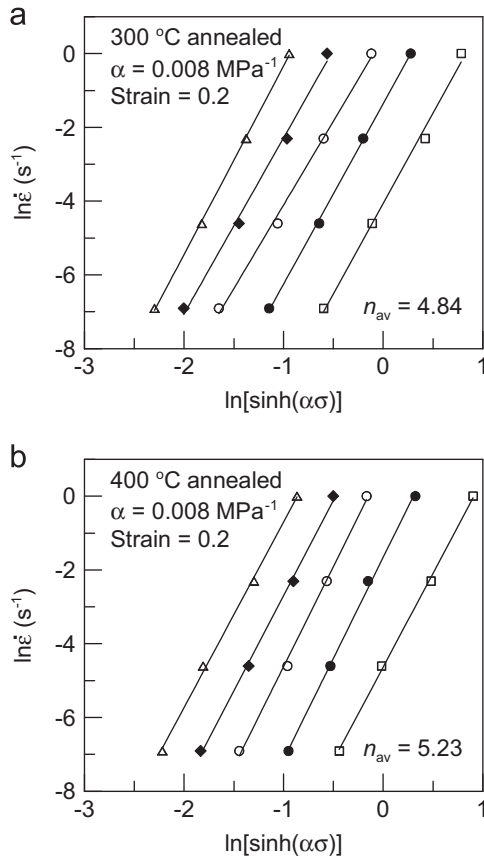
a

b

Fig. 9. Typical plot of $\ln \dot{\varepsilon}$ versus $\ln[\sinh(\alpha\sigma)]$ of the (a) 300 °C annealed and (b) 400 °C annealed specimens at a strain of 0.2 for evaluation of n.

a

b

Fig. 10. Variation in$\ln[\sinh(\alpha\sigma)]$ as a function of reciprocal temperature of the (a) 300 °C annealed and (b) 400 °C annealed specimens at various strain rates and a strain of 0.2.

can be evaluated based on activation energy. By taking the natural logarithms of both sides of Eq. (1), this equation can be rewritten as

$$\ln[\sinh(\alpha\sigma)] = \frac{1}{n}\ln\dot{\varepsilon} + \frac{Q}{nR}\left(\frac{1}{T}\right) - \frac{1}{n}\ln A. \quad (2)$$

The stress multiplier α is an adjustable constant that sets $\alpha\sigma$ into the correct range to make the lines in the $\ln\dot{\varepsilon}$ versus $\ln[\sinh(\alpha\sigma)]$ plot parallel at a particular temperature. Thus, the parallelism of these lines can be evaluated by the standard deviation (STDEV) with respect to the average n. Detailed descriptions of the process used to obtain a suitable α for hyperbolic constitutive analysis are given in previous studies [24,25]. According to Eq. (2), n is the slope of the line in the plot of $\ln\dot{\varepsilon}$ versus $\ln[\sinh(\alpha\sigma)]$ at a given strain and temperature. Rearranging Eq. (2) and differentiating with respect to $1/T$ yields an expression that can be used to calculate the activation energy Q at a given strain and strain rate:

$$Q = R\frac{\partial\ln\dot{\varepsilon}}{\partial\ln[\sinh(\alpha\sigma)]}\bigg|_{\varepsilon,T}\frac{\partial\ln[\sinh(\alpha\sigma)]}{\partial(1/T)}\bigg|_{\varepsilon,\dot{\varepsilon}} \quad (3)$$

The second term on the right side of Eq. (3) refers to the average slope of the lines in the plot of $\ln\dot{\varepsilon}$ versus $\ln[\sinh(\alpha\sigma)]$, whereas the third term refers to the average slope of the lines in the $\ln[\sinh(\alpha\sigma)]$ against $1/T$ plots.
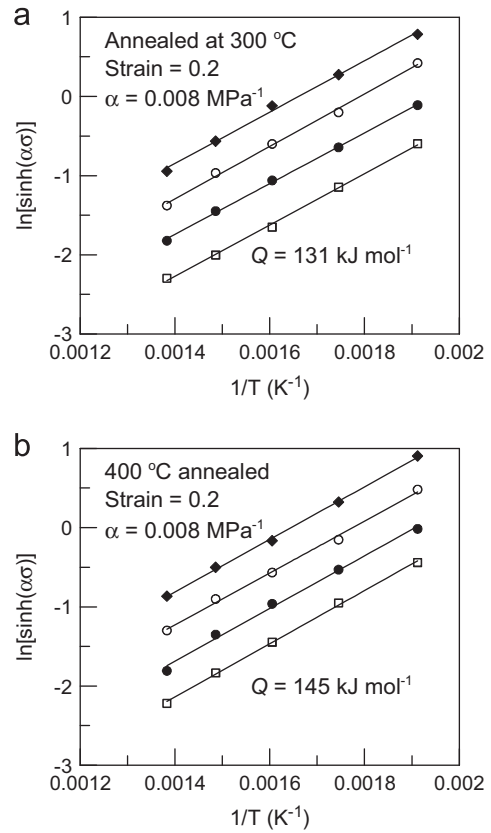
The relationships between the logarithmic stress $\ln[\sinh(\alpha\sigma)]$ and the logarithmic strain rate $\ln\dot{\varepsilon}$ at a strain of 0.2 are given in Fig. 9. The value of the stress multiplier α is equal to 0.008 MPa^{-1}. This value yields the best fit of the experimental data for both annealed specimens. The average values of the stress exponent n are 4.84 with a maximum deviation of 4.3% and 5.2 with a maximum deviation of 3.9% for the 300 and 400 °C annealed specimens, respectively. The average n value of the stress exponent is 4.81 with a maximum deviation of 2.1% using a stress multiplier α of 0.008 MPa^{-1} in the as-extruded specimens [24]. The detailed constitutive analysis of the as-extruded AZ61 Mg alloy has been provided in a previous paper [24]. The n-values suggest that dislocation creep could be a dominant deformation process for the as-extruded and annealed AZ61 Mg alloys [45].

The variation in $\ln[\sinh(\alpha\sigma)]$ as a function of the reciprocal of temperature is given in Fig. 10. The activation energy of the 300 °C annealed specimens estimated using Eq. (3) is 131 kJ mol^{-1}, which is close the value of 135 kJ mol^{-1} for the lattice diffusion in Mg [46]. The activation energy Q of the specimens annealed at 400 °C is 145 kJ mol^{-1}. This value is close to that of 143 ± 10 kJ mol^{-1} for Al diffusion in Mg [47]. The activation energy Q of the as-extruded specimens, which was calculated using Eq. (3), is 127 kJ mol^{-1} [24], a value that is close to that for the lattice diffusion in Mg.

The constitutive equation could be related to the Zener–Hollomon parameter (Z) [48], which is defined as

$$Z = \dot{\varepsilon} \exp\left[\frac{Q}{RT}\right], \tag{4}$$

in which case, Eq. (1) can be shown as

$$Z = A[\sinh(\alpha\sigma)]^n. \tag{5}$$

By taking the natural logarithms of both sides of Eq. (5), the equation can be rewritten as

$$\ln Z = \ln A + n \ln[\sinh(\alpha\sigma)]. \tag{6}$$

Eq. (6) indicates that a linear relation should exist between $\ln Z$ and $\ln[\sinh(\alpha\sigma)]$. The relationships between $\ln Z$ and $\ln[\sinh(\alpha\sigma)]$ for the annealed specimens are given in Fig. 11. The linear relations between $\ln Z$ and $\ln[\sinh(\alpha\sigma)]$ indicate that the relationship of stress with strain rate and temperature at a strain of 0.2 satisfies Eq. (6) well for both annealed specimens. The coefficients of determination R^2 of the fits are 0.998 and 0.998 in the 300 and 400 °C annealed specimens, respectively.

The obtained constitutive parameters at a strain of 0.2 for different initial conditions of AZ61 Mg alloys are summarized in Table 1. The differences in the initial microstructures were found to influence the values of the constitutive parameters. Although all specimens can use the same α to meet the requirement for constitutive analysis, the other constitutive

Table 1
Obtained constitutive parameters at a strain of 0.2 for extruded AZ61 Mg alloys in different initial conditions.

	α (MPa^{-1})	n_z	Q (kJ mol^{-1})	A (s^{-1})
As-extruded [24]	0.008	4.80	127	1.14×10^{11}
300 °C annealed	0.008	4.83	131	2.00×10^{11}
400 °C annealed	0.008	5.23	145	2.51×10^{12}

parameters differ because of variations in the initial conditions. The as-extruded and 300 °C annealed specimens possess comparable initial microstructures and distributions of $Mg_{17}Al_{12}$ particles (Figs. 2 and 3), thus resulting in similar n and Q values. The higher n and Q values obtained in the 400 °C annealed specimen can be attributed to the greater initial grain size and the status of the $Mg_{17}Al_{12}$ particles. The effect of initial grain size on the n value was also observed in AZ31 alloy [49]. Spigarelli et al. [49] reported that the estimated n value of fully annealed extruded AZ31 alloy is higher than that of the as-extruded alloy because of the coarse initial grain size of the annealed alloy. The presence of segregated intermetallic particles in the Mg and Al alloys may give rise to effective barriers opposing the dislocation motion, which should consequently result in a high activation energy value [50,51]. The 400 °C annealed specimen contains markedly less $Mg_{17}Al_{12}$ particles than the 300 °C annealed specimen (Fig. 3) but exhibits higher activation energy. This result indicates that initial grain size has a greater influence than the $Mg_{17}Al_{12}$ particles on the activation energy.

3.4. Strain-dependent constitutive analysis for the 300 °C annealed AZ61 Mg alloy

The evaluation procedure of the constitutive parameters at various strains is the same as that described in Section 3.3. Fig. 12 shows the values of α, n, Q, and A as functions of strain for the specimens annealed at 300 °C. α Decreases with increasing strain, whereas n and A increase with increasing strain. Q does not significantly change with increasing strain. The variations in the constitutive parameters with strain can be related to the stress–strain behavior. A significant increase in flow stress can be observed at low strains under the deformation conditions of high strain rates and low temperatures. As strain increases, the increases in n and A will result in a decrease in flow stress at low strains at a certain strain rate and deformation temperature. Therefore, a sharp decrease in α with increasing strain at low strains compensates for the increases in n and A with increasing strain to satisfy the considerable increase in flow stress on deformation at high strain rates and low temperatures. At strains greater than 0.2, all flow curves exhibit decreasing flow stress after reaching the peak value, as shown in Fig. 5. Thus, the decrease in α with increasing strain is balanced by the increases in n and A with increasing strain to maintain the decline in flow stress in response to dynamic softening.
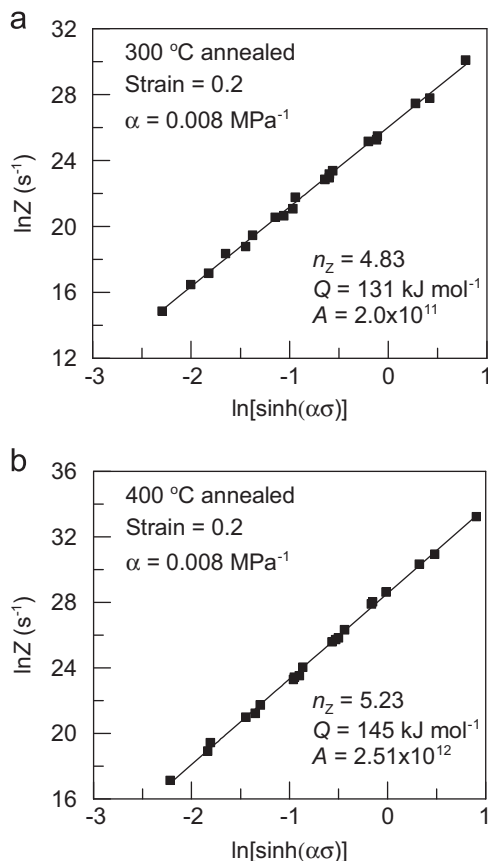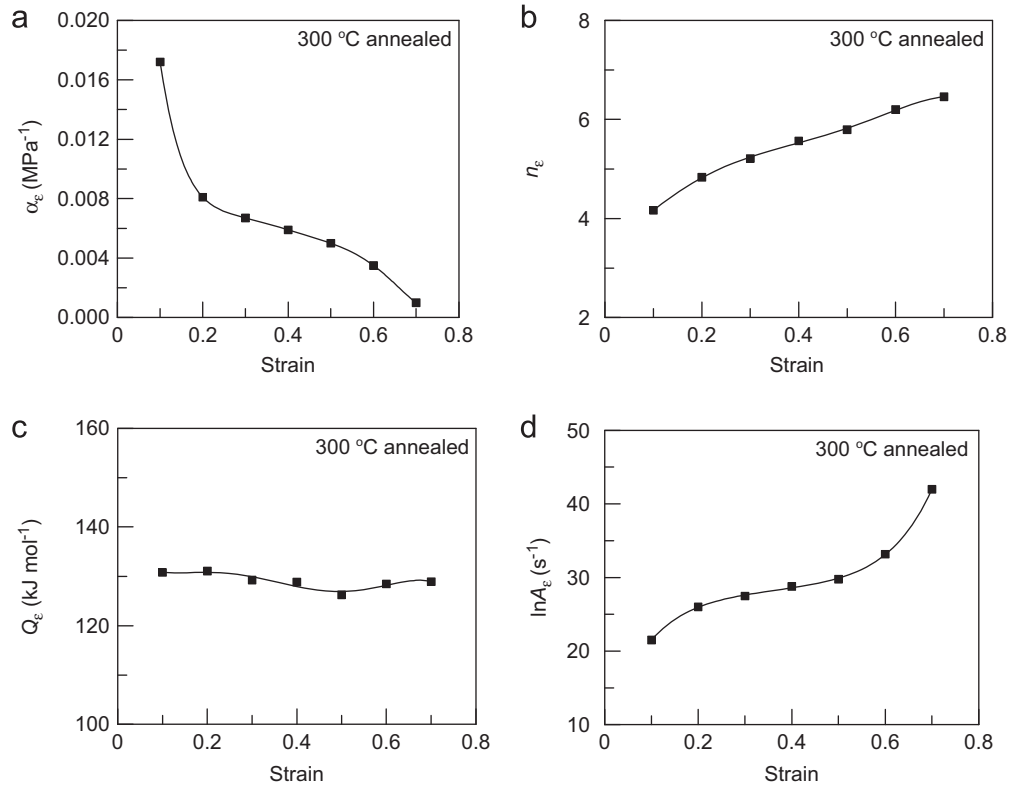

Fig. 11. Variation in $\ln Z$ as a function of $\ln[\sinh(\alpha\sigma)]$ of the (a) 300 °C annealed and (b) 400 °C annealed specimens at various temperatures and a strain of 0.2.

Fig. 12. Variations in constitutive parameters of (a) α value, (b) n value, (c) Q value, and (d) ln A value with true strain of the 300 °C annealed specimens.

Based on the data shown in Fig. 12, polynomial fittings are used to correlate the constitutive parameters with strain in the analysis. Thus, the strain-dependent constitutive equation for 300 °C annealed specimens can be expressed as follows:

$$\dot{\varepsilon} = A_\varepsilon [\sinh(\alpha_\varepsilon \sigma_\varepsilon)]^{n_\varepsilon} \exp\left[\frac{-Q_\varepsilon}{RT}\right] \qquad (7)$$

where

$$\alpha_\varepsilon = 0.0598 - 0.7610\varepsilon + 4.56675\varepsilon^2 - 14.4688\varepsilon^3$$
$$+ 25.2431\varepsilon^4 - 22.9583\varepsilon^5 + 8.4722\varepsilon^6,$$
$$n_\varepsilon = 3.34 + 8.32\varepsilon + 6.93\varepsilon^2 - 87.18\varepsilon^3 + 171.68\varepsilon^4 - 103.62\varepsilon^5,$$
$$Q_\varepsilon = 136.0 - 117.2\varepsilon + 943.1\varepsilon^2 - 3333.3\varepsilon^3 + 5030.6\varepsilon^4 - 2687.0\varepsilon^5,$$
$$\ln A_\varepsilon = 9.41 + 185.81\varepsilon - 821.80\varepsilon^2 + 1983.24\varepsilon^3 - 2527.37\varepsilon^4$$
$$+ 1379.02\varepsilon^5.$$

The polynomial fittings for different constitutive parameters were selected to represent the influence of strain on the constitutive parameters with good correlation. The order of the polynomial fitting for each constitutive parameter was set as low as possible to simplify the equations used to calculate the strain-dependent constitutive parameters. A comparison between the experimental and the predicted flow stresses calculated using Eq. (7) is shown in Fig. 13. The calculated flow stress values are in good agreement with the experimental flow curves. Fig. 13 also shows that different orders of polynomial fittings used for different constitutive parameters should be appropriate for the 300 °C annealed AZ61 Mg alloy.

3.5. Strain-dependent constitutive analysis for the 400 °C annealed AZ61 Mg alloy

Fig. 14 shows the values of α, n, Q, and A as functions of strain for the specimens annealed at 400 °C. The variation in n with strain is similar to that obtained in the specimens annealed at 300 °C, whereas variations in α, Q, and A with strain are notably different from those obtained for the specimens annealed at 300 °C. The decreasing rates of α with respect to strain in the 400 °C annealed specimens are higher than those of the 300 °C annealed specimens at low strains. At high strains, α continues decreasing with increasing strain in the 300 °C annealed specimens, whereas α becomes approximately constant in the 400 °C annealed specimens. At low strains, the rapid decreases in α and Q compensate for the increases in n and A to maintain the increasing flow stress during deformation at high strain rates and/or low temperatures (Fig. 6). As the strains increase from approximately 0.2 to 0.6, the decreasing rates of α and Q decrease, whereas the increasing rates of n and A approach approximately constant rates. The reduced decreasing rates in α and Q are balanced by the near-constant increasing rates in n and A to meet the requirement for the decreasing flow stress after the peak stress is reached. At strains greater than 0.6, a significant decrease in Q with approximately constant n and A is balanced by a slight decrease in α to retain the near-constant stresses for most of the flow curves.

A significant decrease in Q with strain was observed in the 400 °C annealed specimens. Q decreases from approximately
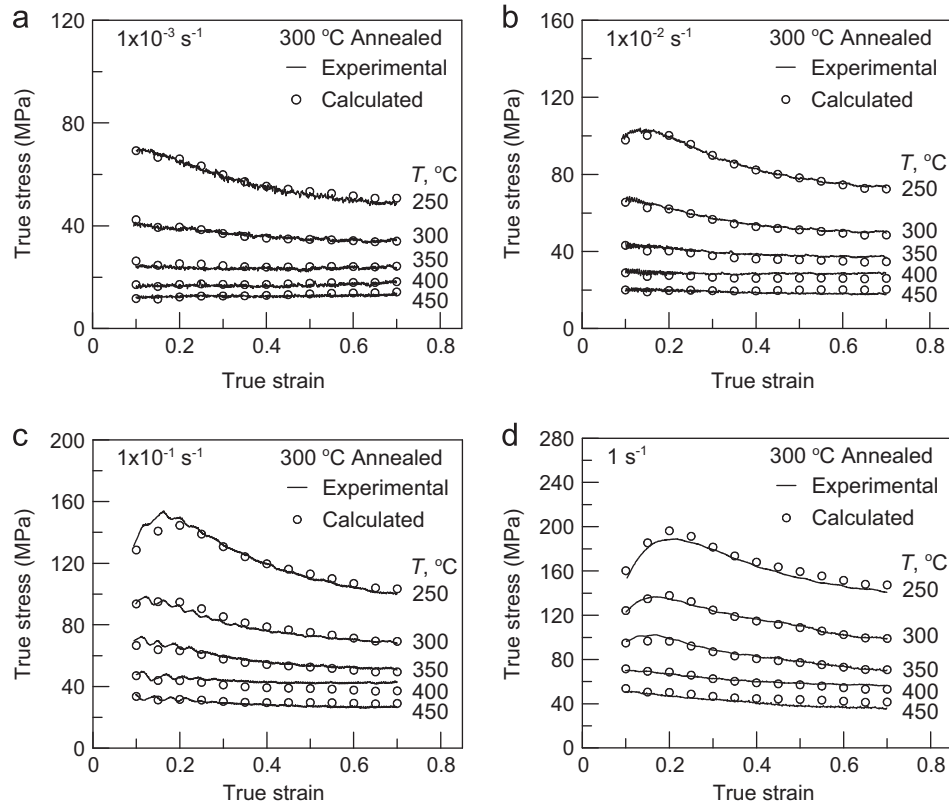
Fig. 13. Experimental and calculated flow stresses of the 300 °C annealed specimen at (a) 1×10^{-3} s^{-1}, (b) 1×10^{-2} s^{-1}, (c) 1×10^{-1} s^{-1}, and (d)1 s^{-1}.

154 kJ mol^{-1} at a strain of 0.1 to approximately 125 kJ mol^{-1} at a strain of 0.7, which indicates that the rate-controlling mechanisms of the 400 °C annealed specimens are Al diffusion at the beginning of deformation and lattice diffusion in Mg at a strain of 0.7. The specimens annealed at 300 °C exhibit a slightly higher Q of approximately 129 kJ mol^{-1} at a strain of 0.7. Q is the rate controlling parameter for hot deformation [45,52] and can vary with strain under non-steady state flow conditions [53]. For glide-controlled dislocation creep, Q is equal to the activation energy for solute diffusion [54]. For grain boundary sliding, Q is equal to the activation energy for lattice diffusion or grain boundary diffusion [55]. Grain boundary sliding is generally observed in materials with a fine grain structure, whereas dislocation creep is observed in materials with a coarse grain structure. Therefore, Q can be related to microstructural evolution during hot deformation. Similar microstructures were observed for both annealed specimens under the same deformation conditions (Fig. 8), thus resulting in similar Q values at a strain of 0.7.

The strain-dependent constitutive parameters for the 400 °C annealed specimens are also treated as polynomial functions of strain. However, the variation of α with strain is unsuitable for fitting by a polynomial function of strain. A power law fitting provides a better result. A power law fitting was therefore selected for strain-dependent α, whereas polynomial fittings were used to correlate the other parameters (n, Q, and ln A) with strain. Consequently, the strain-dependent constitutive equation for the specimens annealed 400 °C can be expressed

as follows:

$$\dot{\varepsilon} = A_\varepsilon [\sinh(\alpha_\varepsilon \sigma_\varepsilon)]^{n_\varepsilon} \exp\left[\frac{-Q_\varepsilon}{RT}\right] \qquad (8)$$

where

$\alpha_\varepsilon = 0.00122\varepsilon^{-1.1893}$,

$n_\varepsilon = 3.61 + 13.69\varepsilon - 39.50\varepsilon^2 + 63.99\varepsilon^3 - 39.10\varepsilon^4$,

$Q_\varepsilon = 181.5 - 426.6\varepsilon + 2040.3\varepsilon^2 - 5448.4\varepsilon^3 + 7324.4\varepsilon^4 - 3849.8\varepsilon^5$,

$\ln A_\varepsilon = 19.87 + 59.62\varepsilon - 85.07\varepsilon^2 - 38.24\varepsilon^3 + 338.37\varepsilon^4 - 305.93\varepsilon^5$.

A comparison between the experimental and the predicted flow stresses calculated using Eq. (8) is shown in Fig. 15. The calculated flow stress values are in good agreement with the experimental flow curves.

3.6. Verification of the developed constitutive equations

To verify the developed constitutive equations for the annealed Mg alloys at elevated temperatures, the flow stresses calculated using Eqs. (7) and (8) are compared with the measured flow stresses, and the results are plotted in Fig. 16. Good correlations exist between the experimental and calculated data obtained for both the 300 and 400 °C annealed specimens. The constitutive equations obtained in this study exhibit a good fit with the measured values. The average absolute relative error (E) values between the calculated flow stress and the experimental flow stress are then calculated to
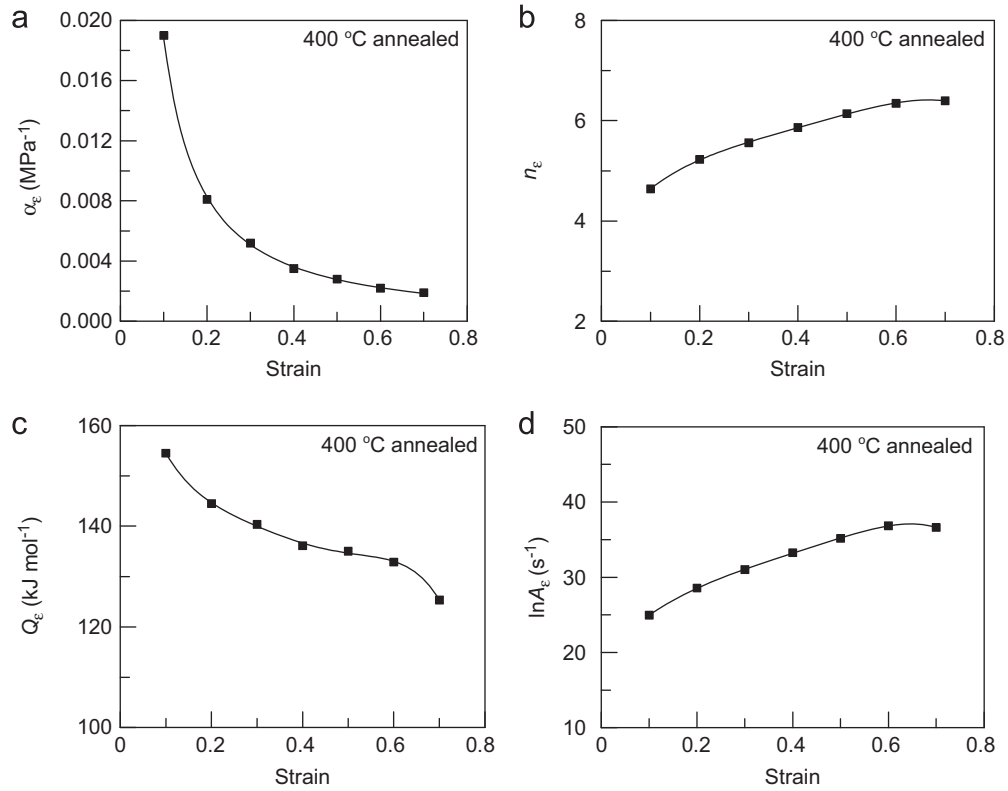
Fig. 14. Variations in constitutive parameters of (a) α value, (b) n value, (c) Q value, and (d) $\ln A$ value with true strain of the 400 °C annealed specimens.
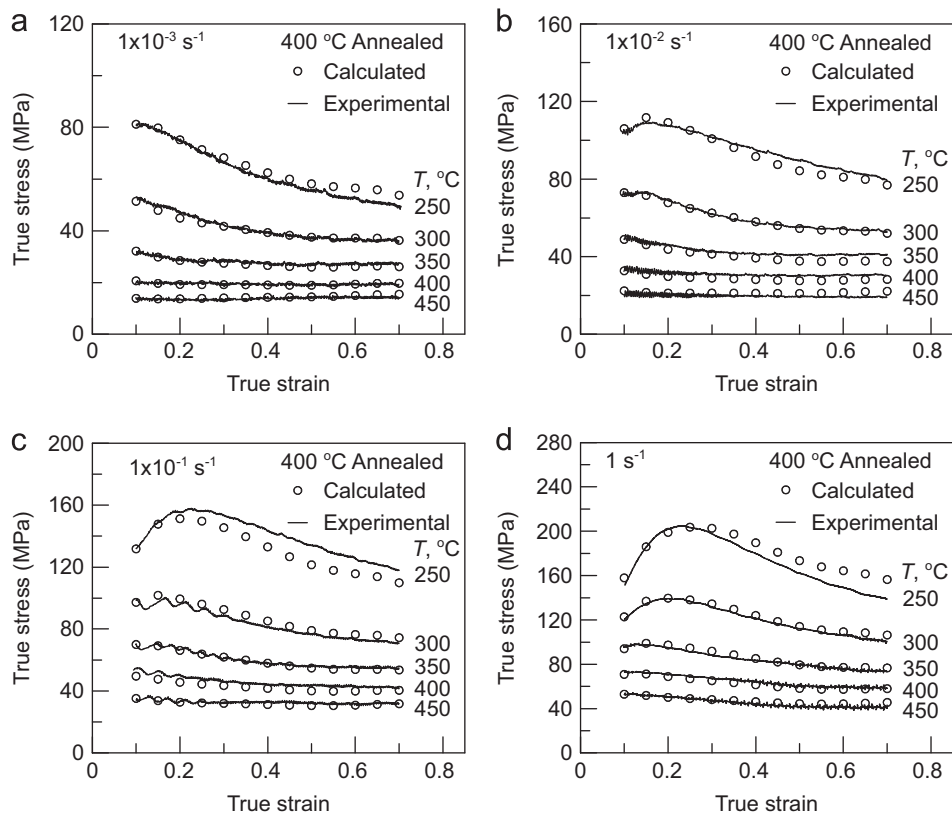

Fig. 15. Experimental and calculated flow stresses of the 400 °C annealed specimen at (a) 1×10^{-3} s^{-1}, (b) 1×10^{-2} s^{-1}, (c) 1×10^{-1} s^{-1}, and (d) 1 s^{-1}.
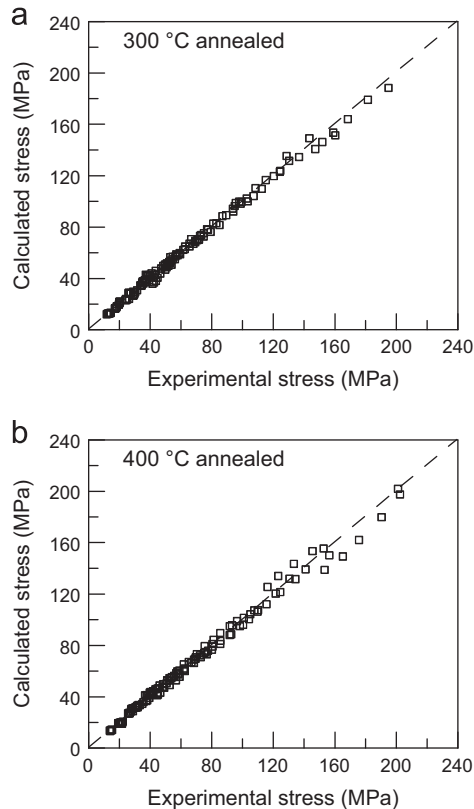
a

b

Fig. 16. Comparisons between the experimental and calculated flow stresses of the (a) 300 °C annealed and (b) 400 °C annealed specimens. The dashed line indicates a perfect match between the measurement and calculation.

evaluate the accuracy of the developed constitutive equations quantitatively. The average absolute relative error (E) is given by

$$E(\%) = \frac{1}{N} \sum_{i=1}^{N} \left| \frac{\sigma_e^i - \sigma_c^i}{\sigma_e^i} \right| \qquad (9)$$

where σ_e is the experimental flow stress, and σ_c is the calculated flow stress obtained from Eqs. (7) or (8). The values of E are approximately 3.73% and 3.82% for the 300 and 400 °C annealed specimens, respectively, which reflect the excellent predictability of the developed constitutive equations. The value of E is approximately 3.99% for the constitutive analysis of the as-extruded Mg alloy [24].

4. Conclusions

In this study, hot compression tests were performed to examine the hot deformation behavior of annealed AZ61 Mg alloys. Constitutive modeling of the flow stress was also conducted. Multiple peak flow behavior was observed in the annealed specimens under the deformation conditions at a strain rate of 1×10^{-1} s^{-1} and at various temperatures. The peak stresses of the 400 °C annealed specimens were higher than those of the 300 °C annealed specimens because of the lower DRX rate in the 400 °C annealed specimens. Constitutive analysis results indicated that the hot deformation behavior of the annealed AZ61 Mg alloys satisfied the hyperbolic-sine

constitutive equation. The influence of strain on the constitutive relation was considered by taking the effect of strain on the constitutive parameters into account. The constitutive parameters of stress multiplier α, stress exponent n, activation energy Q, and constant ln A were calculated by compensating the strain using polynomials in the 300 °C annealed specimens. A power law fitting of α with strain provided better result in the 400 °C annealed specimens, whereas the other constitutive parameters (n, Q, and A) could still be fitted with polynomials. Variations in constitutive parameters with strain were related to the flow behavior. Decreases in α, n, and A as well as increases in Q resulted in an increase in flow stress at a particular strain rate and temperature. The relative absolute error of the calculated stresses compared with the measured stresses in the 300 and 400 °C annealed specimens were 3.73% and 3.82%, respectively, which indicate the excellent predictability of the developed constitutive equations.

References

[1] H. Yoshinaga, R. Horiuchi, Jpn. Inst. Met. 5 (1964) 14–21.
[2] D. Yin, K. Zhang, G. Wang, W. Han, Mater. Sci. Eng. A 392 (2005) 320–325.
[3] R. Panicker, A.H. Chokshi, R.K. Mishra, R. Verma, P.E. Krajewski, Acta Mater. 57 (2009) 3683–3693.
[4] S. Abdessameud, H. Azzeddine, B. Alili, D. Bradai, Trans. Nonferrous Met. Soc. China 10 (2010) 2215–2222.
[5] U.F. Kocks, H. Mecking, Prog. Mater. Sci. 48 (2003) 171–273.
[6] T. Al-Sammana, X. Li, S.G. Chowdhury, Mater. Sci. Eng. A 527 (2010) 3450–3463.
[7] P. Changizian, A. Zarei-Hanzaki, H.R. Abedi, Mater. Sci. Eng. A 558 (2012) 44–51.
[8] N.L. Li, G.J. Huang, R.L. Xin, Q. Liu, Mater. Sci. Eng. A 569 (2013) 18–26.
[9] J.A. del Valle, O.A. Ruano, Mater. Sci. Eng. A 487 (2008) 473–480.
[10] G. Vespa, L.W.F. Mackenzie, R. Verma, F. Zarandi, E. Essadiqi, S. Yue, Mater. Sci. Eng. A 487 (2008) 243–250.
[11] S.W. Xu, S. Kamado, T. Honma, Mater. Sci. Eng. A 528 (2011) 2385–2393.
[12] Y.C. Lin, X.M. Chen., Mater. Des. 32 (2011) 1733–1759.
[13] F.A. Slooff, J. Zhou, J. Duszczyk, L. Katgerman, Scr. Mater. 57 (2007) 759–762.
[14] H.T. Zhou, Q.B. Li, Z.K. Zhao, Z.C. Liu, S.F. Wen, Q.D. Wang, Mater. Sci. Eng. A 527 (2010) 2022–2026.
[15] Y.C. Lin, X.M. Chen, D.X. Wen, M.S. Chen, Comp. Mater. 83 (2014) 282–289Sci 83 (2014) 282–289.
[16] Y.C. Lin, M.S. Chen, J. Zhong, Comp. Mater. Sci. 42 (2008) 470–477.
[17] F.A. Slooff, J. Zhou, J. Duszczyk, L. Katgerman, J. Mater. Sci. 43 (2008) 7165–7170.
[18] F.A. Slooff, J. Zhou, J. Duszczyk, L. Katgerman, Magnesium Technology, TMS, Warrendale, PA, 2007, p. 363–368.
[19] H.Y. Wu, J.C. Yang, J.H. Liao, F.J. Zhu, Mater. Sci. Eng. A 535 (2012) 68–75.
[20] H.Y. Wu, J.C. Yang, F.J. Zhu, H.C. Liu, Mater. Sci. Eng. A 550 (2012) 273–278.

[21] P. Changizian, A. Zarei-Hanzaki, A.A. Roostaei, Mater. Des. 39 (2012) 384–389.
[22] O. Sabokpa, A. Zarei-Hanzaki, H.R. Abedi, N. Haghdadi, Mater. Des. 39 (2012) 390–396.
[23] H. Yu, H.S. Yu, G.H. Min, S.S. Park, B.S. You, Y.M. Kim, Met. Mater. Int. 19 (2013) 651–665.
[24] C.H. Liao, H.Y. Wu, S. Lee, F.J. Zhu, H.C. Liu, C.T. Wu, Mater. Sci. Eng. A 565 (2013) 1–8.
[25] H.Y. Wu, J.C. Yang, F.J. Zhu, C.T. Wu, Mater. Sci. Eng. A 574 (2013) 17–24.
[26] H. Okamoto, J. Phase Equilib. 19 (1998) 598.
[27] H.T. Zhou, A.Q. Yan, C.M. Liu, Trans. Nonferrous Met. Soc. China 15 (2005) 1055–1061.
[28] W. Roberts, Deformation, Processing, and Structure, AMS, Metals Park, Ohio, 1984, p. 109–184.
[29] T. Sakai, J. Mater. Process. Technol. 53 (1995) 349–361.
[30] A. Dehghan-Manshadi, P.D. Hodgson, ISIJ Int. 47 (2007) 1799–1803.
[31] R. Le Gall, J.J. Jonas, Acta Mater. 47 (1999) 4365–4374.
[32] J.J. Jonas, T. Sakai, Deformation, Processing, and Structure, AMS, Metals Park, Ohio, 1984, p. 185–230.
[33] M.J. Luton, C.M. Sellars, Acta Metall. 17 (1969) 1033–1043.
[34] I. Weiss, T. Sakai, J.J. Jonas, Met. Sci. 18 (1984) 77–84.
[35] T. Sakai, J.J. Jonas, Acta Metall. 32 (1984) 189–209.
[36] T. Sakai, M.G. Akben, J.J. Jonas, Acta Metall. 31 (1983) 631–641.
[37] W. Roberts, H. Boden, B. Ahlblom, Met. Sci. 13 (1979) 195–205.
[38] M.M. Myshlyaev, H.J. Mcqueen, A. Mwembela, E. Konopleva, Mater. Sci. Eng. A 337 (2002) 121–133.
[39] T. Al-Samman, G. Gottstein, Mater. Sci. Eng. A 490 (2008) 411–420.
[40] Z.Y. Liu, S. Bai, S.B. Kang, Scr. Mater. 60 (2009) 403–406.
[41] A. Galiyev, R. Kaibyshev, T. Sakai, Mater. Sci. Forum 419–420 (2003) 509–514.
[42] A. Galiyev, R. Kaibyshev, G. Gottstein, Acta Mater. 49 (2001) 1199–1207.
[43] S.E. Ion, F.J. Humphreys, S.H. White, Acta Metall. 30 (1982) 1909–1919.
[44] C. Sellars, W.M. Tegart, Int. Metall. Rev. 17 (1972) 1–23.
[45] H. Somekawa, K. Hirai, H. Watanabe, Y. Takigawa, K. Higashi, Mater. Sci. Eng. A 407 (2005) 53–61.
[46] H.J. Frost, M.F. Ashby, Deformation-mechanism Maps—The Plasticity and Creep of Metals and Ceramics, Pergamon Press, Oxford, 1982.
[47] S.S. Vagarali, T.G. Langdon, Acta Metall. 30 (1982) 1157–1170.
[48] C. Zener, J.H. Hollomon, J. Appl. Phys. 15 (1944) 22–32.
[49] S. Spigarelli, M. El Mehtedi, M. Cabibbo, E. Evangelista, J. Kaneko, A. Jäger, V. Gartnerova, Mater. Sci. Eng. A 462 (2007) 197–201.
[50] Y.V.R.K. Prasad, K.P. Rao, N. Hort, K.U. Kainer, Mater. Lett. 62 (2008) 4207–4209.
[51] H. Zhang, E.V. Konopleva, H.J. McQueen, Mater. Sci. Eng. A 319–321 (2001) 711–715.
[52] H. Watanabe, H. Tsutsui, T. Mukai, M. Kohzu, S. Tanabe, K. Higashi, Int. J. Plast. 17 (2001) 387–397.
[53] M. Suery, B. Baudelet, Rev. Phys. Appl. 13 (1978) 53–66.
[54] O.D. Sherby, M. Burke, Prog. Mater. Sci. 13 (1966) 323–390.
[55] O.D. Sherby, J. Wadsworth, Prog. Mater. Sci. 33 (1989) 169–221.